Manifestation of bound states and coupling to leads in coherent transmission through multiterminal molecular conductors

Alexander Onipko[1,*] and Lyuba Malysheva[1,2]

[1]*Laboratory on Quantum Theory in Linköping, International Society for Independent Research, Box 8017, S-580 08 Linköping, Sweden*

[2]*Bogolyubov Institute for Theoretical Physics, 03680 Kyiv, Ukraine*

(Received 8 May 2012; revised manuscript received 23 July 2012; published 7 August 2012)

We examine analytically a rarely if ever addressed issue: the effects of scattering at the conductor-lead interfaces on the transmittivity of $\mathcal{N}$-terminal molecular conductors. The feeding leads are not one-dimensional and the strength of wire-lead coupling is allowed to be arbitrary. The conductor imbedded into a circuit is supposed to be a Y junction of three identical molecular wires or of two identical wires and one different wire. The wire connector is a C-H group and wires are conjugated and/or saturated oligo(hydro)carbons. The spectrum of branched oligo(hydro)carbons is rationalized in terms of extended and bound states. The junctions, where identical wires are equally coupled to the respective leads (all-symmetric junctions), are compared with hybrid junctions, where nonequivalence of terminal-to-terminal transmission appears due to either not identical wires or not equal coupling, or both. These model systems reveal incredible potentials of branched oligo(hydro)carbons for engineering a variety of molecular electronic devices. In addition, the role of wire connectors, atomic and molecular, is briefly discussed. Some of the obtained results are valid for $\mathcal{N}$-terminal starlike junctions.

DOI: 10.1103/PhysRevB.86.085413 PACS number(s): 72.10.−d, 73.22.−f

I. INTRODUCTION

Miniaturization has become a crucial challenge to be met for further downscaling of electronic devices and circuits.[1–3] This drives a considerable effort aiming to use molecules as active elements of electronic devices, transistors in particular. Many experimental as well as theoretical studies are focused on various realizations of field-effect transistors,[4–9] where the role of one of the transistor terminals is played by a gate electrode. The charge carriers in such devices move from the source to drain electrodes, whereas the gate is closed for the charge transport. In other words, one deals with the two-terminal electron transport. On the other hand, any device inside a molecular-size circuit is a multiterminal, at least a three-terminal, system, where the charge-carrier motion from any in-terminal to any out-terminal occurs coherently. There are not many calculations referring to this kind of devices. Most of them have been based on the Green's-function formalism.[10–12] In a series of articles,[13–15] three- and four-terminal models of logic gates, described by either the tight-binding (TB) or extended Hückel Hamiltonian, have been discussed by using the scattering matrix method. The approximate approaches to the problem have also been developed on the basis of model Hamiltonians[16] and the density-functional theory (DFT) methods as well.[17,18]

As shown recently,[19,20] the starlike junctions of molecular wires exhibit I-V characteristics which contrast those that are known for the same arrangement of conventional resistors. If, for example, the junction is comprised of $\mathcal{N}$ identical molecular wires, as illustrated in Fig. 1, where $\mathcal{N} = 3$, and these wires are equally coupled to the feeding leads, the branched current is proportional to $\mathcal{N}^{-2}$. For this law be valid, all electron pathways inside the junction must be equivalent.

However, Y junctions of not identical wires are of special interest. The wires can be coupled to the respective leads equally or not equally. An analogy with T-shaped and cross-shaped two-dimensional (2D) nanostructures, which are examples of 2D wire junctions, also deserves attention. In particular, the electronic spectrum of such junctions contains bound states that give rise to the transmission resonances at the classically forbidden energies. To our knowledge, the physics of bound states in molecular multiterminal devices has not been addressed yet. These are topics for examination in the present report.

II. FORMAL FRAMEWORK

To study molecular wire junctions exemplified in Fig. 1, we have used the standard formula relating the terminal-to-terminal, energy dependent transmission probabilities $T_{j'j}$, $j, j' = 1,2,\ldots,\mathcal{N}$, to the respective matrix elements of the system Green's function $\mathcal{G}_{j',j}$:[21]

$$T_{j'j} = 4\mathrm{Im}A_j\mathrm{Im}A_{j'}|\mathcal{G}_{j',j}|^2. \tag{1}$$

In this equation, $A_j(E) = V_j^2 G_{1,1}^{\mathrm{lead}\,j}(E)$ with $G_{1,1}^{\mathrm{lead}\,j}$ denoting the (1,1) matrix element of the j-lead Green's function. A_j has the same meaning as the self-energy in the Fisher-Lee-Datta trace formula. This correspondence does not hold, however, in general.[19,20,22]

As known, Eq. (1) has been derived for noninteracting electrons. The effects of electron-electron correlation can essentially modify the transmission of charge carriers and hence the electric performance prescribed by this equation.[23] The development of one-particle theory presented in this study should therefore be considered as a necessary zero approximation that forms the basis for further elaboration.

Usually, Eq. (1) is a starting point to proceed with numerical calculations. But for the given class of molecular devices (which covers the models discussed in Refs. 10–15 as particular cases), matrix $[\mathcal{G}_{j',j}]$ can be expressed in terms of column vector $[G^{\mathcal{M}}_{j',j}] = (G^{\mathcal{M}}_{1,j}\ G^{\mathcal{M}}_{2,j}\ G^{\mathcal{M}}_{j-1,j}\ G^{\mathcal{M}}_{j+1,j}\ G^{\mathcal{M}}_{\mathcal{N},j})^{\mathrm{T}}$ whose components are determined by the matrix elements of the Green's function of the isolated junction $\mathcal{M}$. This vector

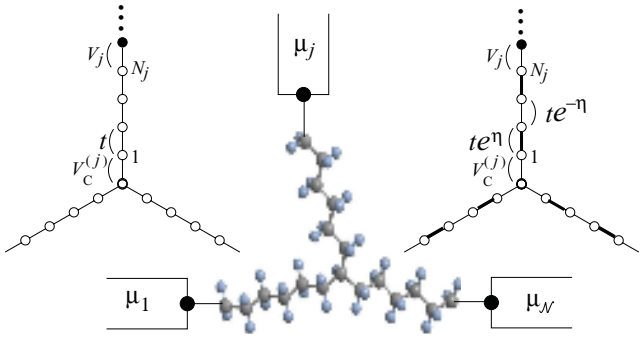

FIG. 1. (Color online) *Ab initio* optimized geometry of junctions of three alkanes and thinkable junction embedments between leads. Geometries of polyene junctions are similar. Both junctions are shown schematically with an indication of system parameters and numbering of carbon atoms (open circles $\overline{1,N_j}$). Binding atoms within leads $j = 1,\ldots,\mathcal{N}$ are shown by black circles.

is subject to matrix equation[19,20]

$$L(j \neq j')[\mathcal{G}_{j',j}] = \left[G^{\mathcal{M}}_{j',j}\right], \tag{2}$$

with

$$L_{j',j''}(j) = \left(1 - A_j G^{\mathcal{M}}_{j,j}\right)\left(\delta_{j',j''} - A_{j''} G^{\mathcal{M}}_{j',j''}\right) - A_j A_{j''} G^{\mathcal{M}}_{j,j'} G^{\mathcal{M}}_{j'',j}. \tag{3}$$

We shall pay most of our attention to Y junctions, $\mathcal{N} = 3$, in which case combining Eqs. (1) and (2) yields[20]

$$T_{2,1} = \frac{4\mathrm{Im}A_1\mathrm{Im}A_2\left|G^{\mathcal{M}}_{1,2}L_{3,3}(1) - G^{\mathcal{M}}_{1,3}L_{2,3}(1)\right|^2}{|L_{3,3}(1)L_{2,2}(1) - L_{3,2}(1)L_{2,3}(1)|^2},$$
$$T_{3,1} = \frac{4\mathrm{Im}A_1\mathrm{Im}A_3\left|G^{\mathcal{M}}_{1,3}L_{2,2}(1) - G^{\mathcal{M}}_{1,2}L_{3,2}(1)\right|^2}{|L_{3,3}(1)L_{2,2}(1) - L_{3,2}(1)L_{2,3}(1)|^2}, \tag{4}$$
$$T_{3,2} = \frac{4\mathrm{Im}A_2\mathrm{Im}A_3\left|G^{\mathcal{M}}_{2,3}L_{1,1}(2) - G^{\mathcal{M}}_{1,2}L_{3,1}(2)\right|^2}{|L_{1,1}(2)L_{3,3}(2) - L_{1,3}(2)L_{3,1}(2)|^2}.$$

Notice that these expressions can be used for any molecular conductor connected to three semi-infinite leads which can be identical or not and may have an arbitrary electronic structure and arbitrary dimensionality. In this sense, the above expressions are more general than any tight-binding transmission formula for three-terminal molecular devices investigated thus far.

Furthermore, provided matrix $[G^{\mathcal{M}}_{j',j}]$ is known, the utilization of Eq. (4) substantially facilitates calculations of transmission probabilities $T_{j'j}$. For instance, the inversion of high-order matrices, which one faces when using the S-matrix description of three-terminal logic gates,[13–15] can be replaced by Eq. (4), where all entries are known. More importantly, for many actual molecular junctions, the analysis of Eq. (4) can be performed analytically.

III. EXTENDED AND BOUND STATES

It is instructive to have a look at the junction electronic structure as it comes out from one-particle Green's function $G^{\mathcal{M}}$. Consider a junction of chainlike wires which are connected with each other via a C-H group (hopping integral $V^{(j)}_{\mathrm{C}}$, see Fig. 1). The end atom of each wire, denoted as N_j, is coupled with the j lead by hopping integral V_j. The matrix elements $G^{\mathcal{M}}_{j',j}$, which enter Eq. (2), refer to different junction sites N_j and $N_{j'}$. They can be expressed in terms of wire Green's function[19]

$$G^{\mathcal{M}}_{N_j,N_{j'}} = \delta_{N_j,N_{j'}} G^{(j)}_{N_j,N_j} + \frac{V^{(j)}_{\mathrm{C}} G^{(j)}_{1,N_j} V^{(j')}_{\mathrm{C}} G^{(j')}_{1,N_{j'}}}{\mathcal{D}_{\{N_j\},\mathcal{N}}}, \tag{5}$$

where

$$\mathcal{D}_{\{N_j\},\mathcal{N}} = E - \sum_{j=1}^{\mathcal{N}} \left[V^{(j)}_{\mathrm{C}}\right]^2 G^{(j)}_{N_j,N_j}. \tag{6}$$

As seen, $G^{\mathcal{M}}$ may have two kinds of poles. One set of poles corresponds to zeros of determinants $D_{\{N_j\}} \equiv \|H^{\{j\}}\|$ which stand for the $\{j\}$ set of isolated N_j-long wires; another one corresponds to zeros of $\mathcal{D}_{\{N_j\},\mathcal{N}}$.

With the reference to Fig. 1 which represents parameters of the respective tight-binding Hamiltonians, let us first discuss starlike junctions composed of either N-long ($N_j = N$) equal-bond, tight-binding chains, $D_{\{N_j\}} \Rightarrow tD_N$, $\mathcal{D}_{\{N_j\},\mathcal{N}} \Rightarrow t\mathcal{D}_{N,\mathcal{N}}$,

$$E = -2t\cos k, \quad D_N(k) = \sin(N+1)k,$$
$$tG^{\mathrm{TB}}_{N,N}(E) = -\frac{\sin(Nk)}{D_N(k)}, \quad tG^{\mathrm{TB}}_{1,N}(E) = -\frac{\sin k}{D_N(k)}, \tag{7}$$
$$\mathcal{D}_{N,\mathcal{N}}(k) = Et^{-1} + \mathcal{N}\sin(Nk)D_N^{-1}(k),$$

or ($N = 2N_d$)-long, tight-binding chains with alternating bonds [polyene (PE) oligomers], $D_{\{N_j\}} \Rightarrow tD_{N_d}$, $\mathcal{D}_{\{N_j\},\mathcal{N}} \Rightarrow t\mathcal{D}_{N_d,\mathcal{N}}$,

$$E^2 = 2t^2(\cosh 2\eta + \cos\xi),$$
$$D_{N_d}(\xi) = e^{-2\eta}\sin(N_d\xi) + \sin[(N_d+1)\xi],$$
$$t^2 G^{\mathrm{PE}}_{2N_d,2N_d}(E) = \frac{E\sin(N_d\xi)}{D_{N_d}(\xi)}, \quad tG^{\mathrm{PE}}_{1,2N_d}(E) = -\frac{e^{\eta}\sin\xi}{D_{N_d}(\xi)},$$
$$\mathcal{D}_{N_d,\mathcal{N}}(\xi) = Et^{-1}\left[1 - \mathcal{N}\sin(N_d\xi)D_{N_d}^{-1}(\xi)\right], \tag{8}$$

where N_d is the number of double bonds. This choice covers the wires with a metallic (gapless) spectrum, Eq. (7), and a semiconductor two-band spectrum with a gap $E_g = 4t\sin\eta$ between the valence and conduction bands, Eq. (8). The derivation of these equations can be found in Ref. 22.

The analysis of the junction spectrum shows that a part of it repeats the spectrum of the respective isolated wire. These are given by poles of $G^{\mathrm{TB}}(E)$: $E_\nu = -2t\cos[\pi\nu/(N+1)]$, $\nu = 1,2,\ldots,N$, or by poles of $G^{\mathrm{PE}}(E)$: $E_\nu = \mp t\sqrt{2(\cosh 2\eta + \cos\xi_\nu)}$, $\nu = 1,2,\ldots,N_d$. The rest of the level energies, denoted henceforth as E_μ, must satisfy equation $\mathcal{D}_{N,\mathcal{N}} = 0$ or $\mathcal{D}_{N_d,\mathcal{N}} = 0$.

Specifically, the spectrum of junctions built up of $(\mathcal{N}-n)$ TB chains and n PE chains is determined by the transcendent equation

$$f_{\mathcal{N},n}(E) = F_n(E), \tag{9}$$

where (for $V^{(j)}_{\mathrm{C}} = t$)

$$f_{\mathcal{N},n}(E) \equiv E/t + \frac{(\mathcal{N}-n)\sin(Nk)}{\sin[(N+1)k]} \tag{10}$$

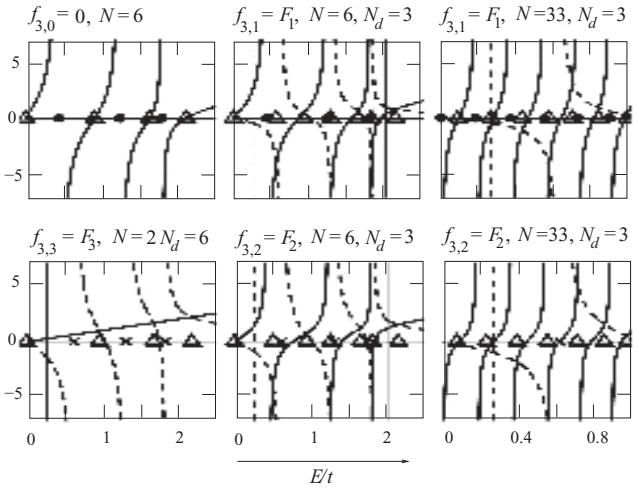

FIG. 2. Energies of μ levels (triangles), given by graphic solutions to equation $f_{3,n}(E) = F_n(E)$ which describes Y junctions with three TB chains ($n = 0$), two TB chains and one PE chain ($n = 1$), one TB chain and two PE chains ($n = 2$), and three PE chains ($n = 3$). Functions $f_{3,n}(E)$ and $F_{n=2,3}(E)$, which are calculated for $\eta = 0.133$, $V_C^{(j)} = t$, are represented by solid and dashed lines, respectively. The chain length is indicated in panel labels. Thin vertical lines indicate the edges of extended states in all-symmetric and hybrid junctions; thin dashed vertical lines indicate the conduction-band bottom of an infinite PE chain. Filled circles and crosses mark energies of ν levels which correspond to an isolated N-long TB chain and a $2N_d$-long PE chain, respectively.

and

$$tF_n(E) \equiv \frac{nE\sin(N_d\xi)}{e^{-2\eta}\sin(N_d\xi) + \sin[(N_d+1)\xi]}, \qquad (11)$$

and where we have used explicit expressions Eqs. (7) and (8) for $D_N(k)$ and $D_{N_d}(\xi)$. In Fig. 2, graphic solutions to Eq. (9) $E = E_\mu$ are marked by triangles.

For the star junctions of identical TB (PE) chains, the energies of μ levels are determined by solutions to equation $f_{\mathcal{N},0}(E) = 0$ [$tF_{n=\mathcal{N}}(E) = E$]. The number of such levels is $N + 1$. The μ levels alternate with $N(\mathcal{N}-1)$ partly degenerate ν levels. These are marked by filled circles and crosses for TB and PE chains, respectively. The level closest to zero-energy is always the ν level ($\mathcal{N}$ independent). The level with the largest energy is always the μ level ($\mathcal{N}$ dependent). For even values of N, equation $f_{\mathcal{N},0}(E) = 0$ has a solution $E = 0$ that appears as a nondegenerate μ level. For odd N, this solution gives the characteristic level of the spectrum of an isolated N-long TB chain. It represents one of the $N(\mathcal{N}-1)$ ν levels. In the symmetric junctions of metallic or semiconducting wires, the zero-energy level corresponds to an extended or local (bound) state, respectively. A conclusion of the above analysis worth mentioning is that the solutions of equations $\mathcal{D}_{N,\mathcal{N}} = 0$ and $\mathcal{D}_{N_d,\mathcal{N}} = 0$ give us only the energies of nondegenerate levels.

The outermost level and its counterpart with negative energy can be located within the band spectrum ($|E|/t \leqslant 2$ for TB-chain junctions and $2\sinh\eta \leqslant |E|/t \leqslant 2\cosh\eta$ for PE-chain junctions) or out of it. This depends on the wire-connector interaction $V_C^{(j)}$, the length and number of wires. If $V_C^{(j)} = t$, we have found that the condition that ensures the existence of bound states reads $N(\mathcal{N}-2) > 2$ for metallic wires and $N_d(\mathcal{N} - 1 - e^{-2\eta}) > 1$ for semiconducting wires.

The first condition obviously excludes bound states in junctions of two metallic wires (an expected result) and may restrict the metallic wire length from below. For instance, if $\mathcal{N} = 3$ or 4, then, for a local out-of-band state to appear N must be not less than 3 or 2.

The second condition allows out-of-band bound states for any value of $\mathcal{N} \geqslant 2$. However, if $\mathcal{N} = 2$ and $\eta = 0.133$,[22] the wire length must be $N = 2N_d \geqslant 10$. If $\mathcal{N} \geqslant 3$, these states are always present in the spectrum of semiconducting-wire junctions. For both types of all-symmetric junctions, composed of either metallic or semiconducting wires, the energy of bound states $E_b^{\pm}$ is practically N independent, if $N \geqslant 10$:

$$E_b^{\pm} = \pm t \begin{cases} 2\cosh\delta_b, & \delta_b = 0.5\ln(\mathcal{N}-1), \\ \sqrt{2(\cosh 2\eta + \cosh\delta_b)}, & \delta_b = \ln(\mathcal{N} - e^{-2\eta}). \end{cases} \qquad (12)$$

Now, let us turn our attention to hybrid Y junctions composed of metallic and semiconducting wires. This case is represented in Fig. 2 by the central and right columns. The upper central panel illustrates the spectra of the Y junction, where two wires have a metal-like spectrum and one has a semiconductorlike spectrum. In the lower central panel, the proportion between the different wires is reversed. We see that the number of solutions to Eq. (9) (triangles) increases from $N + 1 = 7$ for all-symmetric junctions to $2N + 1 = 13$ for hybrid junctions, whereas the energies of N ν levels are determined by solutions to either $D_N(k) = 0$ (panels in the upper row) or $D_{N_d}(\xi) = 0$ (lower row). Thus in the hybrid junctions, the spectrum degeneracy is completely removed. However, the energies of μ and ν levels are so close that the number of resonances in the transmission spectra, Fig. 3, looks like it is the same for all-symmetric and hybrid junctions.

In hybrid junctions with two semiconducting wires and one metallic wire, there can be more than one in-gap state

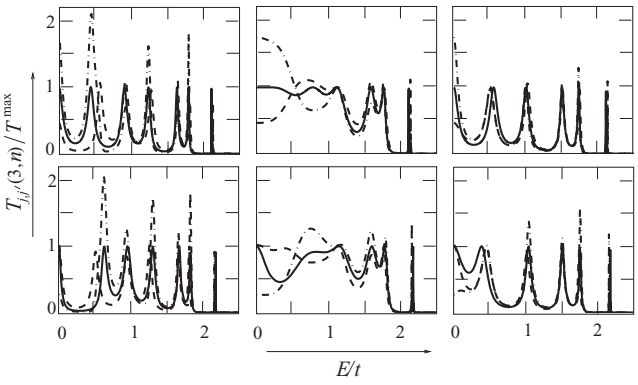

FIG. 3. Transmission spectra of Y junctions $T(3,0)$, $T_{13}(3,1)$, and $T_{12}(3,1)$ in the upper row and $T(3,3)$, $T_{13}(3,2)$, and $T_{12}(3,2)$ in the lower row shown by solid, dashed, and dashed-dotted lines, respectively. Normalization factor $T^{\max} = T^{\max}(3,0) = T^{\max}(3,3) = 4/9$.[19,20] In calculations, $N = 2N_d = 6$, $\eta = 0.133$[22], $V_C^{(j)} = V_j = t$, and the wire-lead coupling is the same for all terminals, $\alpha = 0.2$, 1, and 5 (left, central, and right columns, respectively).

with energies $|E_\mu| < 2t \sinh\eta$. It is clear that these states can no longer be regarded as bound states because all energies $|E| < 2t\cosh\eta$ are allowed. The number of in-gap states increases with the increase of N. To illustrate this point, panels on the right in Fig. 2 represent hybrid junctions with longer TB chains. Four in-gap states are seen instead of only one which is observed in the spectrum of all-symmetric junctions.

One can expect that distinctions between the energy spectra of all-symmetric and hybrid junctions are manifested in the transmission spectra which are to be discussed next.

IV. THROUGH JUNCTION TRANSMISSION

When electron-phonon and electron-electron interactions play a minor role, electrons traveling through a junction of molecular wires can be scattered only at the structure imperfections. For systems in focus, these are the wire-connector and wire-lead interfaces. The resulting effect of the wire-lead coupling on the through junction transmission depends on the connector structure and on how it is connected with the wires. The reverse is also true: the effects on transmission produced by the connector manifest themselves distinctively for equal or not equal wire-lead couplings at different terminals.

The role of wire-lead coupling in junctions with a single-atom connector will be discussed first. Then, a look will be taken at the molecular connectors which already have received some attention in literature but not in the present context.

A. Equal and different wire-lead couplings

In the wide band limit (WBL)[24] that has been often used within the framework of the Landauer approach (see, e.g., Ref. 25 and references therein), the coupling functions are approximated by constants $A_j = -it\alpha_j$. Figure 3 represents the transmission spectra of the hybrid junctions which are calculated in the WBL approximation. The energy dependence of $T_{13}(3,n) = T_{23}(3,n)$ is shown by dashed lines, and transmission probability $T_{12}(3,n)$ is represented by dotted-dashed lines; $n = 1, 2$. Three different values of $\alpha_j = \alpha = 0.2$, 1, and 5 have been used in calculations. For reference, the transmission spectra $T_{j'j}(3,0) \equiv T(\mathcal{N}=3,0)$, $T_{j'j}(3,3) \equiv T(\mathcal{N}=3,3)$ obtained for the same values of α are depicted in Fig. 3 by solid lines.

Analytical forms of $T(\mathcal{N},0)$ and $T(\mathcal{N},\mathcal{N})$ with one coupling constant $\alpha_\mathcal{N}$ distinct from all others read

$$T(\mathcal{N},0) = \frac{4\alpha\alpha_\mathcal{N}\sin^4 k}{|[D_N(k) - i\alpha_\mathcal{N} D_{N-1}(k)][\Pi_{N,\mathcal{N}}(k) - i\alpha\Pi_{N-1,\mathcal{N}}(k)] - i(\alpha-\alpha_\mathcal{N})\sin^2 k|^2},$$

$$T(\mathcal{N},\mathcal{N}) = \frac{4t^2\alpha\alpha_\mathcal{N} e^{4\eta}\sin^4\xi}{\left|\left[tD_{N_d}(\xi) + i\alpha_\mathcal{N} E\sin(N_d\xi)\right]\left\{\Pi_{N,\mathcal{N}}(\xi) + itE^{-1}\alpha\left[e^{2\eta}\Pi_{N_d-1,\mathcal{N}}(\xi) + \Pi_{N_d,\mathcal{N}}(\xi)\right]\right\} - it(\alpha-\alpha_\mathcal{N})e^{2\eta}\sin^2\xi\right|^2}, \quad (13)$$

where $\Pi_{N,\mathcal{N}} \equiv \mathcal{D}_{N,\mathcal{N}}(k)D_N(k)$, $\Pi_{N_d,\mathcal{N}} \equiv \mathcal{D}_{N_d,\mathcal{N}}(\xi)D_{N_d}(\xi)$. Note that the pair of equations above represents the particular cases of the transmission probability expressed in terms of two matrix elements $G^\mathcal{M}_{j,j} \equiv G^\mathcal{M}_d$, $G^\mathcal{M}_{j\neq j',j'} \equiv G^\mathcal{M}_{nd}$. For $\alpha_\mathcal{N} = \alpha$, the corresponding expression, where the wire electronic structure can be arbitrary, has been derived in Ref. 20.

It has been proven that if $A_j = A$ the maximum transmission through $\mathcal{N}$-terminal, all-symmetric junctions equals $4/\mathcal{N}^2$[19]. This result is valid for any junction with transmitting ability at the given energy limited by a single current-carrying state. In particular, these are junctions composed of identical saturated or conjugated oligo(hydro)carbons, oligomers of polyparaphenylene, etc., where either σ- or π-electron transmission dominates. It is seen in Fig. 3 that $\max\{T_{13}(3,1)\} = 4/9$ with a sufficient accuracy, but the maximal value of $T_{12}(3,1)$ is more than two times larger, showing that the latter quantity is close to unity. In other words, in the vicinity of the resonance this three-terminal junction provides nearly a one-way traffic for charge carriers.

In the limit of weak junction-lead coupling $\alpha \ll 1$, the spectra exhibit a sharp resonant structure. Probably, it is somewhat counterintuitive that the resonant structure of the junction transmission spectrum is smoothed out at $\alpha \sim 1$ but not by a strong coupling $\alpha \gg 1$. Since the largest integral transmission is attained for $\alpha \approx 1$, such coupling can be regarded as an optimal contact with the outer electrodes.

The similarity of transmission spectra obtained for the weak and strong coupling of all-symmetric metallic junctions is worth paying attention to. In the WBL approximation, it can rigorously be proved that the central part of the spectrum is not changed if $\alpha \to \alpha^{-1}$. In addition, under these restrictions,

$$T(\mathcal{N},0) = \frac{4}{\mathcal{N}^2}T(2,0). \quad (14)$$

It should be stressed that this simple relation is valid only for star junctions of TB wires.

In the above discussion, the junction-lead coupling was supposed to be equal at all terminals. The effect of coupling asymmetry is illustrated in Fig. 4, where the first two panels in the upper row show the transmission spectra $T_{12}(3,n)$, $T_{13}(3,n)$, $n = 1, 2$ for identical coupling $\alpha_j = 0.2$. Their counterparts in the lower row represent asymmetric coupling $\alpha_1 = \alpha_2 = 5$, $\alpha_3 = 0.2$. As seen, in the vicinity of Fermi energy, $E_F = 0$, the coupling asymmetry results in an appreciable increase of $T_{12}(3,1)$ and decrease of $T_{13}(3,1)$. The associated changes in I-V characteristics can be really impressive. For instance, at a fixed terminal voltage $U_3 = 0$, current $I_2(0 \leqslant U_1 \leqslant U_2)$, calculated according to Büttiker's formula,

$$I_2 = \frac{2e}{h}\sum_{j'=1}^{3}\int_{-\infty}^{\infty} T_{j'2}(E)[f_2(E) - f_{j'}(E)]dE, \quad (15)$$

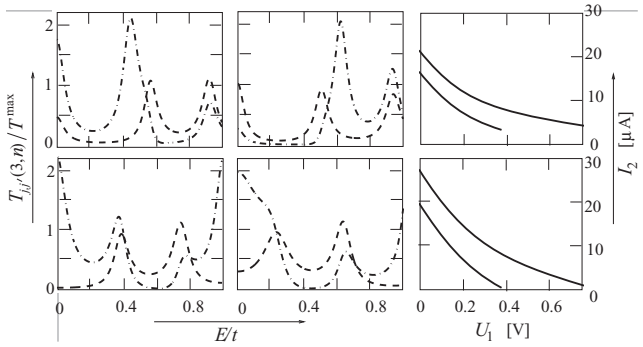

FIG. 4. Left and central columns: Transmission spectra $T_{j'j}(3,1)$ (left) and $T_{j'j}(3,2)$ (central) calculated for the same parameters as in Fig. 3 except that in upper panels $\alpha_j = 0.2$ and in lower panels $\alpha_1 = \alpha_2 = 5, \alpha_3 = 0.2$. The same line styles are used for $T_{13}(3,n)$ and $T_{12}(3,n)$. Right column: Current-voltage characteristics $I_2(0 \leqslant U_1 \leqslant U_2)$, calculated for $n = 1$, $U_3 = 0$, $U_2 = 0.38$ V (shorter curves) and 0.75 V (longer curves).

$f_j = [1 + \exp(\frac{E-eU_j}{kT})]^{-1}$[26] exhibits a five-times variation for equal couplings, and more than 30- and 60-times variation for not equal couplings, if the terminal voltage U_2 is fixed at ≈0.7 and 0.4 V, respectively (right column in Fig. 4). Calculated for zero and room temperatures, these I-V curves are practically indistinguishable.

By varying the wire length, I-V characteristics of Y junctions can be obtained in any subvoltage range. The replacement of the carbon-atom connector by nitrogen or another heteroatom changes the transmission spectrum (and hence I-V curves) quite radically. Also, changing the value of reference voltage U_3 and the terminal of its application results in a variety of different I-V curves. Since the DFT calculations show branched oligo(hydro)carbons as essentially plane molecules (see Fig. 1) they can be physisorbed on a substrate to be contacted electrically. Taken together these properties of branched oligo(hydro)carbons make them very attractive for a diversity of well-predictable device applications.

B. Effect of connector

Equations (1)–(4) relate through junction transmission probabilities to the Green's function that describes the molecular complex composed of a molecule plus wires attached to it. Following this design, $G^{\mathcal{M}}$ can be defragmented into the wire and connector Green's functions, G^0 and $G^{\rm c}$, by using the Dyson equation

$$G^{\mathcal{M}}_{m,m'} = G^0_{m,m'} - \sum_{m'',m'''} G^0_{m,m''} V_{m'',m'''} G^{\mathcal{M}}_{m''',m'}, \qquad (16)$$

where V is the connector-wire interaction matrix. The solution gives an expression of $G^{\mathcal{M}}_{m,m'}$ for needed atomic coordinates n_j and $n_{j'}$, as a functional of related matrix elements $G^0_{m_i,m'_i}$, $G^{\rm c}_{p_i,p'_i}$, and V_{m_i,p_i}.

For the symmetric and hybrid Y junctions similar to that exemplified in Fig. 5, the system of equations to solve

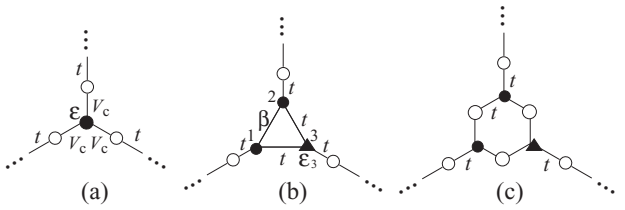

FIG. 5. Tight-binding models of atomic (a) and molecular (b) and (c) connectors. Site energy of unfilled circles is zero. Correspondence with notations used in Ref. 13: $\varepsilon = \varepsilon_3 \equiv \omega$, $V_{\rm c} \equiv \alpha$, $t \equiv h$.

reads

$$\begin{aligned} G^{\mathcal{M}}_{1_1,m} &= G^0_{1_1,m} - G^0_{1_1,1_1}\left(tG^{\mathcal{M}}_{1_3,m} + \beta G^{\mathcal{M}}_{1_2,m}\right), \\ G^{\mathcal{M}}_{1_2,m} &= G^0_{1_2,m} - G^0_{1_2,1_2}\left(tG^{\mathcal{M}}_{1_3,m} + \beta G^{\mathcal{M}}_{1_1,m}\right), \\ G^{\mathcal{M}}_{1_3,m} &= G^0_{1_3,m} - tG^0_{1_3,1_3}\left(G^{\mathcal{M}}_{1_1,m} + G^{\mathcal{M}}_{1_2,m}\right), \end{aligned} \qquad (17)$$

where $G^0_{1_i,1_i}$ denotes the wire Green's-function matrix element which refers to the i wire first site and which, at the same time, is the ith site of the molecular connectors in Figs. 5(b) and 5(c). The meaning of coordinate indices is easily understood by considering the forthcoming examples. In these examples, we shall concentrate exclusively on the explicit analytical results. These can be obtained for one-dimensional (1D) leads only.

1. Heteroatom connector

As known, finding the solution to the Lippman-Schwinger equation often suggests a useful alternative to the scheme of calculations enclosed in Eqs. (1)–(4). For a single-atom scatterer characterized by the site energy ε and resonant interaction V_j with the nearest atom of j wire 1_j, the general expression for the wire j to wire j' transmission probability can be obtained straightforwardly. It reads

$$T^{\infty}_{jj'} = \frac{V_j^2 V_{j'}^2 \left|G_{1_j}(k_j) G_{1_{j'}}(k_{j'})\right| \mathcal{F}(k_j,k_{j'})}{\left|E - \varepsilon - \sum_{j''=1}^{\mathcal{N}} V_{j''}^2 G^{(j'')}_{1_{j''},1_{j''}}(k_{j''})\right|^2}, \qquad (18)$$

where $E = E(k_j)$ is the dispersion relation for the j wire, $G_{1_j}(k_j)$ stands for the prefactor in $G^{(j)}_{1_j,1_j} = G_{1_j}(k_j)e^{ik_j n}$,

$$\mathcal{F}(k_j,k_{j'}) = \frac{|\psi^0_{1_j}(k_j)\psi^0_{1_{j'}}(k_{j'})|}{|\psi^{\infty}_{1_j}(k_j)\psi^{\infty}_{1_{j'}}(k_{j'})|}, \qquad (19)$$

$\psi^0_{n_j}(k_j) = \psi^{\infty}_{1_j}(k_j)e^{-ik_j n}$ − complex conjugate describes the superposition of incident and reflected waves in the semi-infinite 1D wire $\mathrm{M}^{(j)}_1$-$\mathrm{M}^{(j)}_2$-. . . with identical monomers $\mathrm{M}^{(j)}_n = M^{(j)}$, $n = 1,2,\ldots$, and $\psi^{\infty}_{n_j}(k_j) = \psi^{\infty}_{1_j}(k_j)e^{ik_j n}$ is an electron wave propagating over equivalent 1_j sites in the infinite 1D wire . . .-$\mathrm{M}^{(j)}$-$\mathrm{M}^{(j)}$-. . . . To emphasize the academic character of this and similar models of multiterminal transmission the respective transmission probabilities are marked by label ∞.

An interesting particular case of a nonsymmetrical Y junction was discussed by Ami and Joachim.[13] Using the TB wire model defined in Eq. (7), they noticed that if $\varepsilon = 0$, $V_{j=1,2} = t/\sqrt{2}$, and $V_{j=3} = t$, the transmission $3 \to 1 = 3 \to 2$ occurs without backscattering, that is, $T^{\infty}_{13} = T^{\infty}_{23} = 0.5$.

For junctions with arbitrary numbers $\mathcal{N} - n$ and n referring to TB and PE wires, which are equally coupled with the

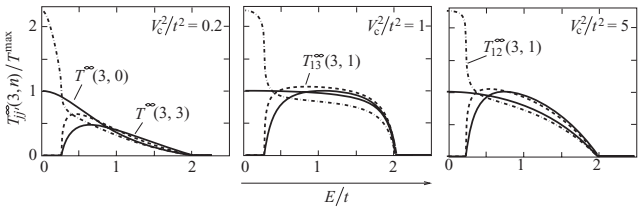

FIG. 6. Transmission probabilities for Y junctions formed by different 1D leads connected with a single-atom connector, Eq. (20). The ratio of the resonance-transfer interaction between the connector and leads V_c to the value of t serves as a panel labeling, $\varepsilon = 0$. The correspondence between line styles and junction types is the same as in Figs. 3 and 4.

connector, the dependence of transmission coefficients on energy can be represented in an explicit form:

$$T_{j'j}^{\infty}(\mathcal{N},n) = \frac{4V_c^4}{\left|tE(E-\varepsilon)+(\mathcal{N}-n)V_c^2Ee^{ik}-ntV_c^2(1+e^{2\eta}e^{i\xi})\right|^2} \times \begin{cases} E^2\sin^2 k, & n=0\ (\mathrm{TB}\to\mathrm{TB}) \\ t^2e^{4\eta}\sin^2\xi, & n=3\ (\mathrm{PE}\to\mathrm{PE}) \\ tEe^{2\eta}\sin\xi\sin k, & n=1,2\ (\mathrm{TB}\leftrightarrow\mathrm{PE}). \end{cases} \quad (20)$$

It is fundamentally important that Eq. (20) takes into account an unavoidable mismatch between site energies and hopping integrals in different wires. The mismatch mentioned enters the transmission probability via dispersion relations $E = \varepsilon_{\mathrm{TB}} - 2t\cos k$ and $(E-\varepsilon_{\mathrm{PE}})^2 = 2\beta^2(\cosh 2\eta + \cos\xi)$. In Fig. 6, these parameters are set to be equal, which is not realistic. It is easy to foresee the main qualitative changes in the presented transmission spectra, which correspond to nonzero values of $\beta - t$ and/or $\varepsilon_{\mathrm{PE}} - \varepsilon_{\mathrm{TB}}$. However, the instructive quantitative estimates require reliable values of these parameters. This is a disputable subject, far beyond the scope of this work.

The effect of mismatch between the site energies of the connector and wires is also included explicitly into Eq. (20). For the star junction shown in Fig. 5(a), the transmission probability $T_{j'j}^{\infty}(\mathcal{N},0) \equiv T^{\infty}(\mathcal{N},0)$ is equal to

$$T^{\infty}(\mathcal{N},0) = \frac{V_c^4(4-E^2/t^2)}{t^2(E-\varepsilon)^2 - \mathcal{N}V_c^2E(E-\varepsilon) + \left(\mathcal{N}V_c^2\right)^2}, \quad (21)$$

or, in the particular case $\varepsilon = 0$,

$$T^{\infty}(\mathcal{N},0)|_{\varepsilon=0} = \frac{4}{\mathcal{N}^2}\frac{1-E^2/(4t^2)}{1-\frac{E^2}{\mathcal{N}^2V_c^4}\left(\mathcal{N}V_c^2-t^2\right)}. \quad (22)$$

An equivalent formula for the reflection coefficient in the Y junction, $R^{\infty}(3,0) = 1 - 2T^{\infty}(3,0)$, was obtained in Ref. 13.

It immediately follows from Eq. (21) that any nonzero ε shifts the energy of the transmission maximum from $E_{\max} = 0$ to

$$E_{\max} = \frac{2t^2\varepsilon}{2t^2 - \mathcal{N}V_c^2}. \quad (23)$$

Also, it is obvious that if $\varepsilon = 0$ and $V_c^2 = 2t^2/\mathcal{N}$ the transmission is maximal for all energies, $T^{\infty}(\mathcal{N},0)(E)|_{\varepsilon=0} = 4/\mathcal{N}^2$. The authors of the above-quoted paper[13] have come to the same conclusion. However, they stated it without the proof of its validity for an arbitrary number of wires.

Figure 6 visualizes the dependence of transmission on the ratio V_c^2/t^2 (an analog of coupling parameter α) as well as the difference between all-symmetric and hybrid junctions of the type in Fig. 5(a). As long as the perturbation parameters remain small, $\varepsilon, V_c^2/t^2 \ll 1$ (in practice < 0.2), the transmission spectra for these junctions undergo no qualitative changes.

Specifying the latter statement for the junctions of TB wires, the transmission spectrum does have a maximum $\max\{T^{\infty}(\mathcal{N},0)\} = 4/\mathcal{N}^2$, if the junction parameters satisfy the following conditions:

$$\frac{V_c^2}{t^2} < \frac{2-|\varepsilon|}{\mathcal{N}}, \quad \text{if} \quad \frac{V_c^2}{t^2} < \frac{2}{\mathcal{N}},$$

or

$$\frac{V_c^2}{t^2} > \frac{2+|\varepsilon|}{\mathcal{N}}, \quad \text{if} \quad \frac{V_c^2}{t^2} > \frac{2}{\mathcal{N}}.$$

Otherwise, such a maximum does not exist.

The data presented above are far from exhausting the rich physics that the model of junctions of semi-infinite wires actually contains. However, as emphasized above this model has little to do with the transmission of real junctions which are in contact with the outer electrodes. One can see a drastic disagreement with the predictions that take into account the presence of wire-lead interfaces. The corresponding transmission spectra are depicted in the upper row in Fig. 3.

2. *Cyclopropane connector*

Figure 5(b) specifies parameters of the tight-binding Hamiltonian for a three-site connector. With all equal site energies and hopping integrals, it corresponds to the tight-binding model of cyclopropane. The Green's-function matrix elements needed to describe this connector according to Eq. (16) are the following:

$$G_{m,1_1}^{\mathcal{M}}D_{\mathcal{M}} = -tG_{1_1,1_1}^0G_{n,1_3}^0 + \frac{G_{m,1_1}^0\left(1-t^2G_{1_1,1_1}^0G_{1_3,1_3}^0\right) - G_{m,1_2}^0G_{1_1,1_1}^0\left(\beta - t^2G_{1_3,1_3}^0\right)}{1-\beta G_{1_1,1_1}^0}$$

$$G_{m,1_2}^{\mathcal{M}} = G_{m,1_1}^{\mathcal{M}}|_{m,1_1\leftrightarrow m,1_2},$$

$$G_{m,1_3}^{\mathcal{M}}D_{\mathcal{M}} = (1+\beta G_{1_1,1_1}^0)G_{m,1_3}^0 - tG_{1_3,1_3}^0(G_{m,1_1}^0 + G_{m,1_2}^0), \quad (24)$$

where $D_{\mathcal{M}} = 1 + \beta G_{1_1,1_1}^0 - 2t^2G_{1_1,1_1}^0G_{1_3,1_3}^0$. Combined with Eq. (4), the above equation includes as particular cases all models of three-terminal molecular devices discussed in Ref. 13.

The equation above can be used in two ways. The first is to substitute it into Eq. (16). This gives the Green's function $G^{\mathcal{M}}$ for the molecular complex consisting of cyclopropane, two identical wires attached to sites 1 and 2, and a different wire attached to site 3. In this case, $G_{m,1_j}^0$ has the meaning of the matrix elements of wire ($m = 1_i, i = 1,2,3$) or connector ($m = i = 1,2,3$) Green's functions. For oligomers M-M-...-M with a variety of monomers M, the needed expressions of $G_{m,1_j}^0$ are collected in Ref. 22.

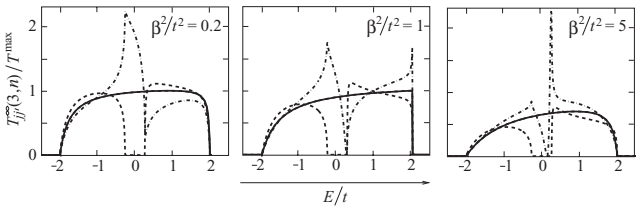

FIG. 7. Transmission probabilities for Y junctions formed by different 1D wires that are connected with a propanelike connector shown in Fig. 5(b) and described by Eq. (25) with $\varepsilon = \varepsilon_3 = 0$. Solid lines correspond to three TB wires; dashed (T_{31}) and dashed-dotted (T_{21}) lines correspond to the case of two TB wires and one PE wire, the latter connected with site 3. Panels are labeled by the values of β^2/t^2 used in calculations.

The second is to use in this equation $G^0_{m,1_{1,2}} = \delta_{m,1_{1,2}}(E-\varepsilon)^{-1}$ and $G^0_{m,1_3} = \delta_{m,1_3}(E-\varepsilon_3)^{-1}$. In this case, Eq. (24) determines the Green's function for the cyclopropane connector:

$$
\begin{aligned}
G^{\mathrm{c}}_{1,1} &= G_{2,2} = \frac{(E-\varepsilon)(E-\varepsilon_3)-t^2}{(E-\varepsilon-\beta)D_{\mathrm{c}}},\\
G^{\mathrm{c}}_{1,2} &= \frac{-\beta(E-\varepsilon_3)+t^2}{(E-\varepsilon-\beta)D_{\mathrm{c}}},\\
G^{\mathrm{c}}_{3,3} &= \frac{1}{D_{\mathrm{c}}}(E-\varepsilon+\beta), \quad G^{\mathrm{c}}_{1,3} = G^{\mathrm{c}}_{2,3} = -\frac{t}{D_{\mathrm{c}}},
\end{aligned}
\tag{25}
$$

where $D_{\mathrm{c}} = (E-\varepsilon)(E-\varepsilon_3)+\beta(E-\varepsilon_3)-2t^2$.

As an application of this equation, Fig. 7 represents the transmission spectra that are calculated with the use of $G^{\mathrm{c}}_{j,j'}$ instead of $G^{\mathcal{M}}_{j,j'}$ in Eq. (4) and coupling functions $A_1 = A_2 = -V_{\mathrm{c}}^2 e^{ik}/t$ and $A_3 = V_{\mathrm{c}}^2(1+e^{i\xi+2\eta})E^{-1}$.

These calculations show that the use of a propane molecule as a connector (central panel) might be of practical interest because of the strongly asymmetric transmission spectrum in the vicinity of Fermi energy. This asymmetry clearly originates from the asymmetry of the propane electronic spectrum. It is further enhanced by the interference effects, if $\beta > t$. However, the realization of propane-based Y junctions is questionable. One reason is that cyclopropane is chemically unstable. Another hindrance for the synthesis may arise because of steric constraints.

3. *Annulene connector*

The annulene connector, where the binding atoms form an equilateral or isosceles triangle, can be treated similarly. For example, the probability of transmission through an all-symmetric Y junction, where three semi-infinite TB chains are coupled with carbon atoms and these binding atoms are separated from each other by N-long carbon chains, takes the form

$$
T^{\infty} = \frac{4\left(t/V_c^2\right)^2 \sin^2 k \left(G^{\mathrm{c}}_{1,2}\right)^2}{\left|\left(t/V_c^2\right)e^{-ik}+G^{\mathrm{c}}_{1,1}-G^{\mathrm{c}}_{1,2}\right|^2\left|\left(t/V_c^2\right)e^{-ik}+G^{\mathrm{c}}_{1,1}+2G^{\mathrm{c}}_{1,2}\right|^2},
\tag{26}
$$

where $E = -2t\cos k = \varepsilon - 2t\cos\bar{k}$, ε is the site energy within the annulene ring, and

$$
\begin{aligned}
tG^{\mathrm{c}}_{1,1} &= \frac{1}{2}\frac{\cos[3(N+1)\bar{k}/2)}{\sin\bar{k}\sin[3(N+1)\bar{k}/2]},\\
tG^{\mathrm{c}}_{1,2} &= \frac{1}{2}\frac{\cos[(N+1)\bar{k}/2]}{\sin\bar{k}\sin[3(N+1)\bar{k}/2]}.
\end{aligned}
\tag{27}
$$

The case of a benzene connector, $N = 1$, has received a good deal of attention in literature,[12,27,28] where it appeared as a molecule in a direct contact with the electrodes. A doubtful value of the TB chain model for the electrodes is already mentioned. In general, any direct electric contact of a roughly 0.5-nm-size molecule is hardly possible because of proximity effects. From this point of view, the use of large carbon cycles for modeling the electronic device functions is preferable. Thereby, Eq. (26) can be used for orienting estimates. An efficient and rigorous way of a sensible modeling of Y junctions with an account for unavoidable scattering at the junction-lead interfaces is suggested by Eqs. (1)–(4) and (17). Concrete implementations of this scheme for junctions with the molecular connectors will be reported in future publications.

V. CONCLUSION

We have addressed several issues which are important for the understanding of advantages of multiterminal molecular electronic devices and difficulties of their implementation. Molecular complexes, where chainlike molecules are coupled with a heteroatom or some molecular connector and thus the complex forms a Y junction, are a sort of solvable problem for chemists. The crucial issue is the controlled electric contact with three outer electrodes. The wire soldering to the molecule physisorbed on the surface substrate[29] might well be a breakthrough. Yet, it is long way to the goal. A tremendous research effort is required that has to be justified. It is our hope that this work adds to the driving force of such effort. Shown to be an inherent property of hybrid junctions, which allows us to switch the current direction by changing the applied voltage at different terminals, it can be used for many device applications of molecular circuits. A number of other useful properties of different Y junctions can be read in the presented transmission spectra. They reveal the potentials of symmetric and nonsymmetric junctions which depend on how the wires are connected with the electrodes. The derivation of these results has demonstrated the efficiency of Green's-function defragmentation for molecular device modeling and can serve as a guide for a variety of other applications.

ACKNOWLEDGMENTS

This and the preceding article (Ref. 20) would not appear without the support that A. O. received from October 2011 to July 2012 from Ingemar Lagerlöf, Annika Erlandsson, Yvonne Landberg, Josefin Kronqvist, Thomas Gustafsson, and many others at Universitetssjukhuset (University Hospital) in Linköping. Partial financial support from the Visby program of the Swedish Institute is gratefully acknowledged.

*aleon@ifm.liu.se

[1] A. Nitzan and M. A. Ratner, Science **300**, 1384 (2003).
[2] N. J. Tao, Nature Nanotechnology **1**, 173 (2006).
[3] F. Chen and N. J. Tao, Acc. Chem. Res. **42**, 429 (2009).
[4] C. Joachim, J. K. Gimzewski, and A. Aviram, Nature (London) **408**, 541 (2000).
[5] S.-H. Ke, W. Yang, and H. U. Baranger, Nano Lett. **8**, 3257 (2008).
[6] A. F. Young and P. Kim, Nature Physics **5**, 222 (2009).
[7] F. Zahid, M. Paulsson, E. Polizzi, A. W. Ghosh, L. Siddiqui, and S. Datta, J. Chem. Phys. **123**, 064707 (2005).
[8] H. Song, Y. Kim, Y. H. Jang, H. Jeong, M. A. Reed, and T. Lee, Nature (London) **462**, 1039 (2009).
[9] M. Galperin, M. A. Ratner, A. Nitzan, and A. Troisi, Science **319**, 1056 (2008)
[10] L. Wang, K. Tagami, and M. Tsukada, Jpn. J. Appl. Phys. **43**, 2779 (2004).
[11] P. Dutta, S. K. Maiti, and S. N. Karmakar, Organic Electronics **11**, 1120 (2010).
[12] S. K. Maiti, Solid State Commun. **150**, 1269 (2010).
[13] S. Ami and C. Joachim, Phys. Rev. B **65**, 155419 (2002).
[14] R. Stadler, S. Ami, M. Forshaw, and C. Joachim, Nanotechnology **13**, 424 (2002); **14**, 722 (2003).
[15] R. Stadler, S. Ami, C. Joachim, and M. Forshaw, Nanotechnology **15**, S115 (2004).
[16] B. G. Cook, P. Dignard, and K. Varga, Phys. Rev. B **83**, 205105 (2011).
[17] K. K. Saha, B. K. Nikolić, V. Meunier, W. Lu, and J. Bernholc, Phys. Rev. Lett. **105**, 236803 (2010).
[18] K. K. Saha, T. Markussen, K. S. Thygesen, and B. K. Nikolić, Phys. Rev. B **84**, 041412(R) (2011).
[19] L. Malysheva and A. Onipko, Phys. Status Solidi B **248**, 2676 (2011).
[20] A. Onipko and L. Malysheva, Phys. Rev. B **86**, 045457 (2012).
[21] S. Datta, *Electronic Transport in Mesoscopic Systems* (Cambridge University Press, Cambridge, 1995).
[22] A. Onipko and L. Malysheva, in *Nano and Molecular Electronics Handbook* (CRC Press, Boca Raton, 2007), Chap. 23, pp. 1–38. This reference contains a good deal of information which is relevant to this work and spread over quite a number of papers.
[23] Y. Meir and N. S. Wingreen, Phys. Rev. Lett. **68**, 2512 (1992); G. Kolesov and Y. Dahnovsky, Adv. Quantum Chem. **61**, 261 (2011).
[24] A. Prociuk, B. Van Kuiken, and B. D. Dunietz, J. Chem. Phys. **125**, 204717 (2006).
[25] C. Herrmann, G. C. Solomon, J. E. Subotnik, V. Mujica, and M. Ratner, J. Chem. Phys. **132**, 024103 (2010).
[26] M. Büttiker, Phys. Rev. Lett. **57**, 1761 (1986).
[27] D. M. Cardamone, C. A. Stafford, and S. Mazumdar, Nano Lett. **6**, 2422 (2006).
[28] C. A. Stafford, D. M. Cardamone, and S. Mazumdar, Nanotechnology **18**, 424014 (2007).
[29] Y. Okawa, S. K. Mandal, C. Hu, Y. Tateyama, S. Goudecker, S. Tsukamoto, T. Hasegava, J. K. Gimzevski, and M. Aono, J. Am. Chem. Soc. **133**, 8227 (2011).